Encryption/decryption and microtarget capturing by pH-driven Janus microstructures fabricated by the same femtosecond laser printing parameters

OPEN ACCESS
IOP Publishing | IMMT
International Journal of Extreme Manufacturing
Int. J. Extrem. Manuf. **3** (2021) 025001 (9pp)
https://doi.org/10.1088/2631-7990/abe092

Encryption/decryption and microtarget capturing by pH-driven Janus microstructures fabricated by the same femtosecond laser printing parameters

Zhaoxin Lao[1,2,4], Rui Sun[3,4], Dongdong Jin[1,4], Zhongguo Ren[2], Chen Xin[2], Yachao Zhang[2], Shaojun Jiang[2], Yiyuan Zhang[2] and Li Zhang[1]

[1] Department of Mechanical and Automation Engineering, The Chinese University of Hong Kong, Sha Tin, Hong Kong, People's Republic of China
[2] CAS Key Laboratory of Mechanical Behavior and Design of Materials, Key Laboratory of Precision Scientific Instrumentation of Anhui Higher Education Institutes, Department of Precision Machinery and Precision Instrumentation, University of Science and Technology of China, Hefei, Anhui 230027, People's Republic of China
[3] Chengdu Fine Optical Engineering Research Center, Chengdu 610041, People's Republic of China

E-mail: lizhang@mae.cuhk.edu.hk

Received 8 September 2020, revised 13 October 2020
Accepted for publication 26 January 2021
Published 16 February 2021

Abstract

Several natural organism can change shape under external stimuli. These natural phenomena have inspired a vast amount of research on exploration and implementation of reconfigurable shape transformation. The Janus structure is a promising approach to achieve shape transformation based on its heterogeneous chemical or physical properties on opposite sides. However, the heterogeneity is generally realized by multi-step processing, different materials, and/or different processing parameters. Here, we present a simple and flexible method of producing pH-sensitive Janus microactuators from a single material, using the same laser printing parameters. These microactuators exhibit reversible structural deformations with large bending angles of $\sim 31^{\circ}$ and fast response ($\sim$0.2 s) by changing the pH value of the aqueous environment. Benefited from the high flexibility of the laser printing technique and the spatial arrangements, pillar heights, and bending directions of microactuators are readily controlled, enabling a variety of switchable ordered patterns and complex petal-like structures on flat surfaces and inside microchannels. Finally, we explore the potential applications of this method in information encryption/decryption and microtarget capturing.

Supplementary material for this article is available online

Keywords: micro actuator, smart material, pH hydrogel, Janus structure, laser printing

(Some figures may appear in colour only in the online journal)

1. Introduction

After sufficient evolution, a variety of natural organisms, especially plants, have gained the ability to change their shapes in response to various external stimuli [1–5]. For example, the scales of seed-bearing pine cones move in response to changes in relative humidity, releasing the cone's seeds in

[4] These authors contributed equally to this work.

2631-7990/21/025001+9$33.00

dry environments [1]. Benthic octopuses and cuttlefish have the unique capability to dramatically and quickly change their skin's texture from smooth and flat to rough [2]. The Venus flytrap can rapidly close its leaves when it encounters external stimuli [3]. Inspired by these natural behaviors, researchers have undertaken considerable efforts to realize reconfigurable shape transformation in a controlled manner. For example, laser-induced self-growing reversible architectures [6] based on shape-memory polymers suggest potential applications for microparticle capture/release. Self-folding robots that represent both complex structures and functional devices have been built [7–13]. Capillary force is also used in self-assembly processes to form orderly, hierarchical structures, showing invertible shape deformation [14–19].

The Janus structure, which has two different types of chemical or physical properties on opposite sides [20], is a promising candidate for achieving shape transformation. Janus structures have attracted increasing attention owing to their wide applications, ranging from medical therapy [21] and environmental engineering [22, 23] to microrobotics [24] and sensors [25]. So far, Janus structures have been developed to implement shape transformation under diverse external stimuli [25–29]. For example, Janus polyurethane acrylate nanofibers processed by sputter deposition of palladium at an incident ion beam angle of 45° exhibit reversible structural deformation when exposed to hydrogen [25]. Smart humidity-driven anisotropic graphene oxide/reduced graphene oxide bilayer structures have been fabricated by unilateral UV irradiation of graphene oxide papers [26]. Reversible, thermally- and optically-responsive polymer/SWNT bilayer actuators have been realized by vacuum filtering a single-walled carbon nanotube solution through a 10 μm thick polycarbonate membrane [27]. However, current Janus structures require multiple supplementary processes and different processing parameters during fabrication [30, 31], such as sputter deposition [25], UV irradiation [26], or electron beam irradiation [28] to break the symmetry, which are time-consuming and costly. Moreover, most Janus structures are formed with different materials [32], which leads to extra expenditures and additional challenges (e.g. mismatch and adhesion). Besides, most Janus structures have uniform deformation in an array, which makes it difficult to customize their structural orientation within a certain range and results in a lack of flexibility.

In this work, we develop a simple and flexible method to fabricate pH-driven geometry-switchable Janus microactuators by a dual-scanning femtosecond (fs) laser. Janus micropillars are polymerized from pH-sensitive hydrogel, whose volume changes based on the pH value. When the pH is less than 9, the hydrogel microstructure shrinks, otherwise, it swells. More subtly, such dual-scanning employs the same laser parameters, but heterogeneous polymerized pillars form spontaneously due to the laser beam scattering on the first printed structure. The two sides of these Janus micropillars expand at different rate when the pH value changes, leading to invertible bending of the entire Janus micropillar. Owing to the high flexibility of the laser printing technique [33, 34], the spatial arrangements, heights, and bending directions of these Janus micropillars can be manipulated. Consequently, a variety of surface patterns including complex petal-like structures can be fabricated, tuned, and reverted on flat substrates and inside microchannels. As a proof-of-concept demonstration, the Janus microactuators were employed as a serviceable tool for information encryption/decryption and trapping of microparticles, suggesting their promising interdisciplinary value in the fields of smart display, microobject manipulation, filtration, and transportation.

2. Result and discussion

2.1. Fabrication of Janus micropillars by dual-scanning strategy

As schematically represented in figure 1(a), micropillars were fabricated by focusing an fs laser beam (with a wavelength of 800 nm and pulse duration of 75 fs) into a pH-sensitive hydrogel, using an objective lens (Olympus, 50×, NA = 0.8). The sample was mounted on a 3D nanotranslation stage (PI, E727) to determine the pillars' locations and heights. When the distance (0.15 μm) between two micropillars was less than the diameter of a single round micropillar, the two micropillars became one micropillar with an elliptical cross-section. Therefore, we can process micropillars by exposing them twice in adjacent positions, termed dual-scanning. In our previous works [33, 35, 36], we found that the expansion ratio of the hydrogel is directly related to the laser exposure dosage for photopolymerization. In figure 1(a), the black side of the pillar was printed first and the grey side was printed second with the same processing parameters. Due to the laser beam scattering effect of the first printed structure, the second printed structure (grey side) was less polymerized than the first printed structure (black side), leading to the spontaneous formation of heterogeneity in micropillar.

Photo-crosslinked hydrogel micropillars contain polymeric backbones with ionic pendant groups, which ionize and develop fixed charges in the polymer network, generating the electrostatic repulsive forces responsible for pH-dependent swelling or deswelling [33, 34, 36, 37]. Small changes around the critical pH can significantly change the mesh size of the polymeric networks. The pendant groups of the anionic hydrogels used in this work were un-ionized below and ionized above the pH threshold (pH = 9) of the polymeric network. As a result, the hydrogel swelled when pH > 9 because of the high osmotic swelling force of ions. The volume change property of the structure is closely related to the laser processing dosage. The lower laser power results in weaker extent of polymerization which will lead to lower resistance to swelling force caused by the change of pH values. Therefore, the microstructures obtained with lower laser power have larger expansion. On the contrary, higher laser power brings in lower expansion ratio of polymerized structures. Therefore, Janus micropillars with two sides with different expansion ratios can be readily obtained with our simple dual-scanning strategy. Since a circular micropillar was processed after the first exposure, the light scattering effect of the existing structure reduced the laser power during the second exposure. Therefore, even if the same laser power is used for the dual-scanning process,

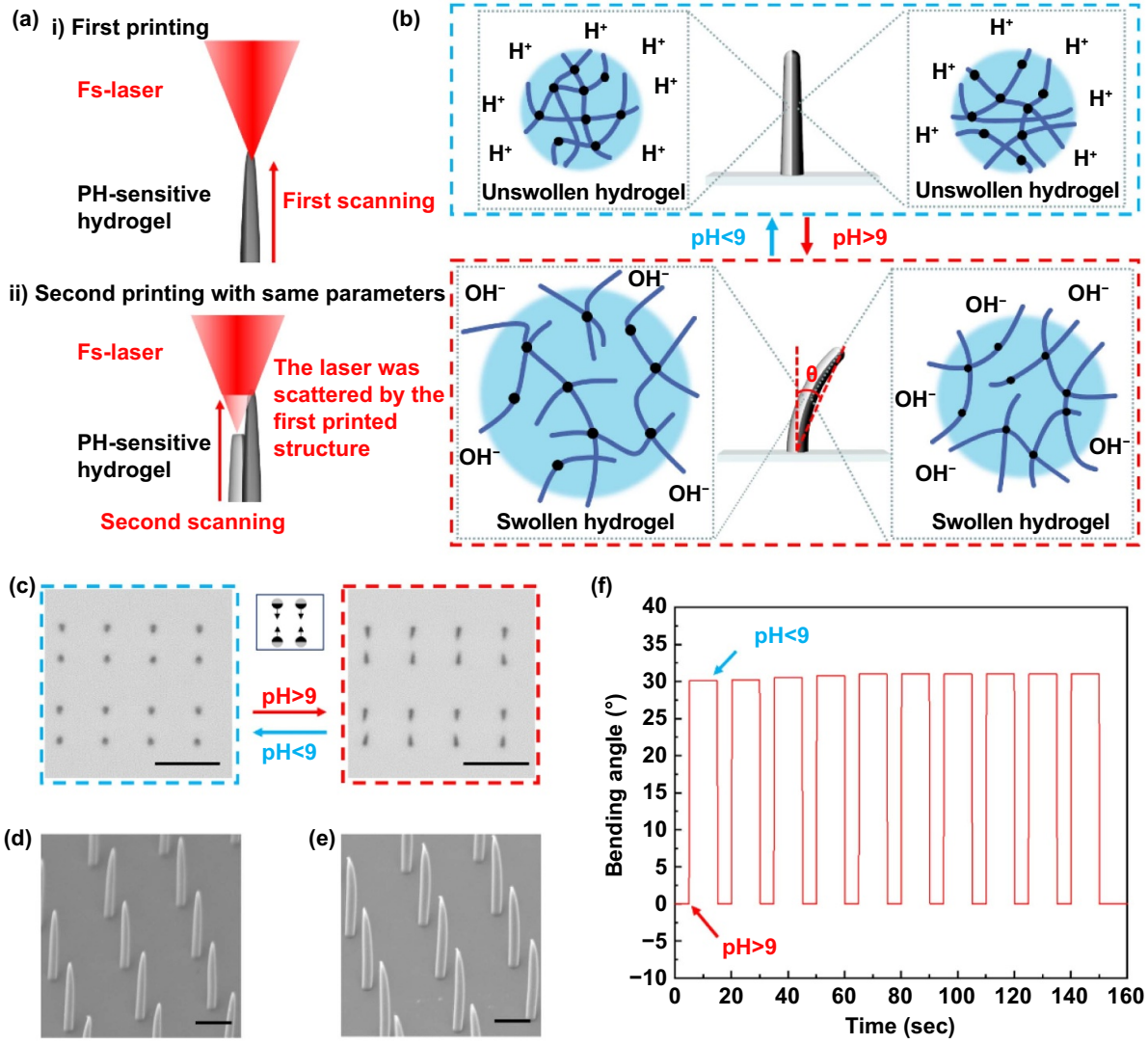

Figure 1. Janus micropillars fabricated by fs laser dual-scanning. (a) Schematic illustration of the laser printing of Janus micropillars. The black side was printed first and the grey side was printed second with the same processing parameters. The parts were printed close enough together that a single pillar formed after dual-scanning. Because the light scattering by the first printed structure, the second printed structure (grey side) was less polymerized than the first printed structure (black side) so that heterogeneity formed spontaneously. (b) Schematic illustration of Janus micropillar's bending and straightening effects. (c) Optical micrographs of the Janus micropillars under different pH environments. Scale bars: 15 μm. (d), (e) SEM images of ordinary micropillars by single exposure and Janus micropillars by dual-scanning. Scale bars: 4 μm. (f) Repeatability of shape transformation response of Janus micropillars upon pH change.

the power used in the second processing is relatively lower than the first. Thus, the Janus micropillar bends in the direction of the part obtained in the first exposure. Our dual-scanning fabrication is much easier than traditional fabrication methods because the same laser parameters are used throughout the entire process. It is noteworthy that the pH value of the aqueous environment around the micropillars during the fabrication process is less than 9. The contraction effect in an acidic environment is not significant. Therefore, the micropillar recovers to its original straight position when pH < 9. As shown in figure 1(b), the Janus micropillars with two different colors were fabricated by dual-scanning. The black part represents the first exposure area and the gray part represents the second. According to the above analysis, the micropillars are in a straight state when pH < 9, as the unswollen hydrogels on two sides have the same volume. When the pH value exceeds 9, the hydrogel in the second exposure (gray) area expands more than that in the first exposure area (black), so the micropillar bends in the direction of the part obtained by the first exposure. Figure 1(c) shows the optical micrographs of 'two-pillars' structures in straight and bent states. The inset of figure 1(c) shows the pattern, in which the black semicircles represent the position of the first exposure, and the gray semicircles represent the position of the second exposure. The arrows represent the expected bending direction of the micropillar when the solution's pH exceeds 9. Scanning electron microscope (SEM) images of single exposed micropillars and double exposed Janus micropillars are shown in figures 1(d) and (e). The geometry of the micropillars obtained by our dual-scanning closely resemble the geometries of micropillars obtained by a

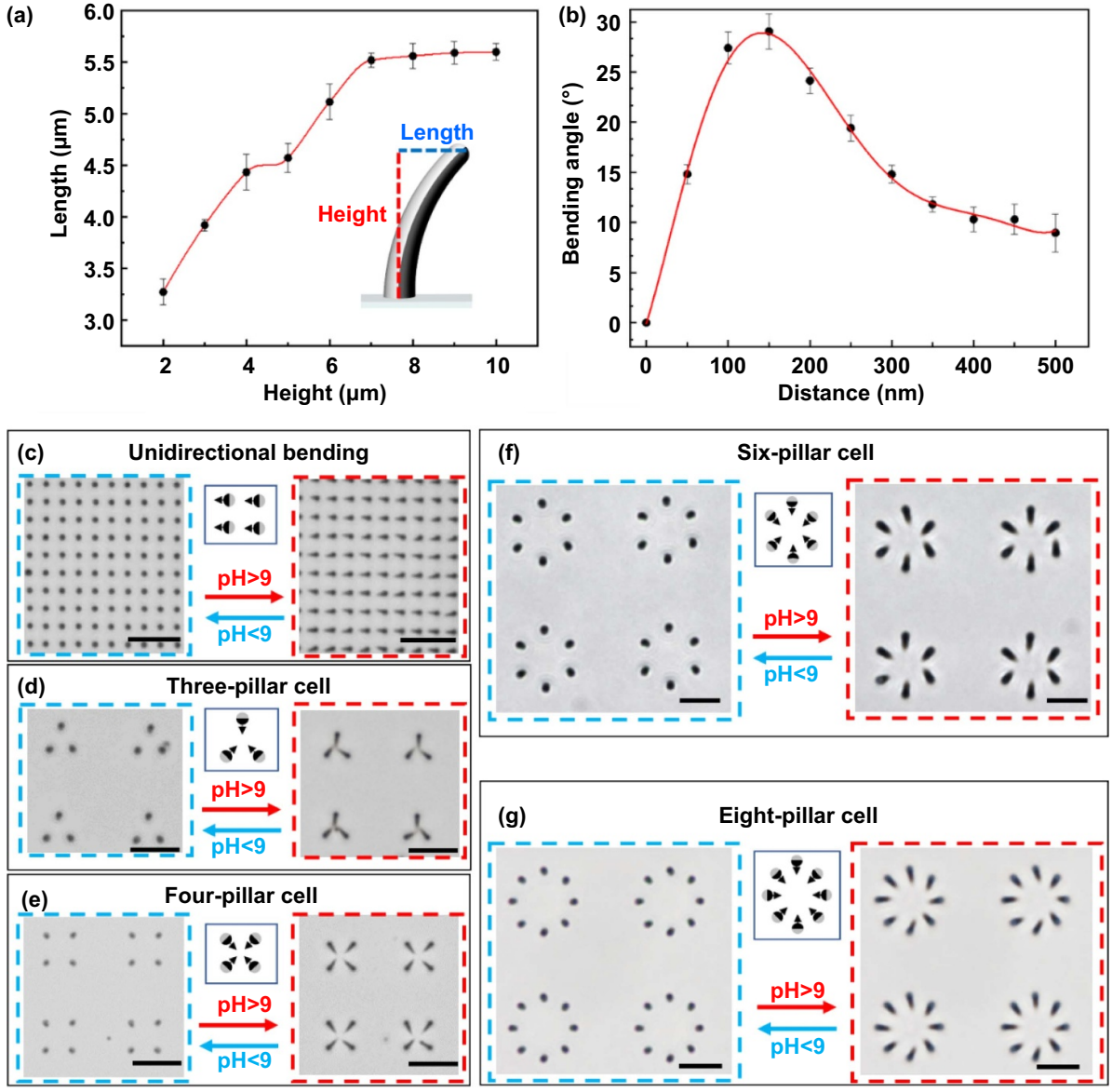

Figure 2. Fabrication of highly controllable Janus micropillars. (a) The quantitative relationship between the length of the bent micropillar and the height of the straight micropillar. (b) The quantitative relationship between the bending angle of micropillar and the distance between the dual-scanning positions. (c) Array of Janus micropillars capable of unidirectional bending. (d)–(g) Janus micropillar arrays composed of three, four, six, and eight micropillars bending to the center of the pattern. All scale bars: 15 μm.

single exposure. The dual-scanned micropillars have slightly larger diameters. The Janus micropillars remained stable and did not show signs on degradation during multiple cycles of bending and recovering (figure 1(f)). The process of changing shape takes about only 0.2 s (SI video 1 (available online at stacks.iop.org/IJEM/3/025001/mmedia)) and the maximum bending angle (θ, the site at which we measure the angle is shown in the inset of figure 1(b)) is about 31°.

2.2. Realization of patterns with multielement cells and petal-like structures

The length of the bent micropillar, in the top view, increases with its growth height until it reaches 7 μm (figure 2(a)). When the height exceeds 7 μm, the length of micropillars in the top view remains stable, indicating that bending only occurs at the top of the micropillars. We also investigated the quantitative relationship between the bending angle of micropillar and the distance between the dual-scanning positions (figure 2(b)). The bending angle reaches its peak when the distance between the scanning positions is about 150 nm. The bending angle gradually decreases as the distance increases above 150 nm.

Owing to the high flexibility of the laser printing technique, more complex patterns can be achieved based on the dual-scanning approach. By controlling the processing position and sequence of the two exposures, the number of pillars, spatial location, and bending direction can be easily controlled. A variety of ordered patterns can be constructed as a block of Janus micropillars, which can bend and return to a straight state by tuning the pH value. Figures 2(c) and (g)

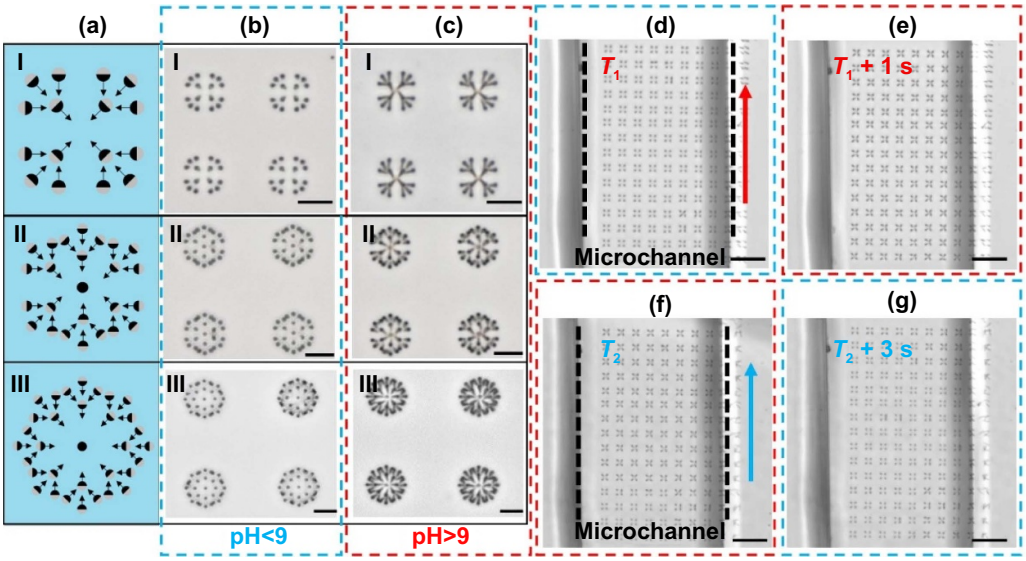

Figure 3. Complex petal-like microstructures fabricated by fs laser dual-scanning. (a) Schematics of printing designs using 16 (I), 25 (II), and 33 (III) pillars. (b), (c) Optical micrographs of symmetric hierarchical networks when (b) pH < 9 and (c) pH > 9. Scale bars: 15 μm. (d)–(g) pH-driven microactuator array in microchannels under pH < 9 (d), (g) and pH > 9 (e), (f) respectively. The red and blue arrows respect the diffusion direction of added pH > 9 and pH < 9 solutions. As the solution diffuses in the channel, the microactuators in the array respond very quickly. Scale bars: 50 μm.

show a series of patterns with multielement cells. The Janus micropillars were in an initially straight state when the pH value was less than 9. When we raised the pH value above 9, all of the micropillars bent in the same direction, which was determined by the sequence of the dual-scanning processes. This pH-driven shape transformation can be repeated many times, exhibiting significant invertibility and stability. The optical micrographs of the Janus micropillar arrays with three- (figure 2(d)) and four-pillar cells (figure 2(e)) show fine replication results and high uniformity of the dual-scanning process. Six-pillar cell arrays with hexagonal arrangement and eight-pillar cell arrays with octagon arrangement were also designed (figures 2(f) and (g)).

Complex petal-like structures can also be fabricated by deliberately setting micropillars with specific bending directions in a pattern. Figure 3(a) shows the conceptional designs by intentionally varying the local position and the bending directions of Janus micropillars in a large cell to create desired hierarchical structures. Figure 3(b) (pH < 9) and (c) (pH > 9) show that complex petal-like structures can be realized on the basis of the design. We can see that the Janus micropillars bend and assemble in the expected directions to form the desired patterns. Moreover, we also fabricated and tested microactuator arrays formed from Janus pillars in channels (figures 3(d) and (g)), which highlights the flexibility of this fabrication method. The red and blue arrows indicate the diffusion direction of pH > 9 and pH < 9 solutions. As the pH > 9 solution diffuses in the channel, all of the microactuators in the array changed from upright to curved in 1 s. On the contrary, returned to upright positions in 3 s as the pH < 9 solution diffused through the array. The differences between the recovery times of the array were dominated by the pH changes caused by the diffusion of the solution, rather than the responding time of the individual Janus micropillar. (More details can be seen in SI Video 3.)

2.3. Applications of the pH-driven Janus microactuator arrays

Here we explore the possible applications of the pH-driven Janus microactuator arrays in information encryption and decryption. As mentioned above, the bending direction of the Janus microactuator can be controlled arbitrarily by controlling the dual-scanning parameters. We can utilize microactuators with different bending directions to display particular information, similar to nixie tube, which can present complex information with simple graphics and patterns. Moreover, the Janus microactuators straighten when pH < 9, remaining the same as the ordinary micropillars fabricated by a single exposure process. Based on this phenomenon, information can be encrypted and decrypted by changing the pH value. Figure 4(a) shows the design approach of this information encryption/decryption method. Circles with single black color represent the ordinary micropillars fabricated by single exposure, and dichromatic circles represent the Janus microactuators. The arrows indicate the expected bending directions of these Janus microactuators. Information can be displayed when the pH of solution increases (the right of figure 4(a)). The encryption and decryption of the Arabic numerals '1234' at different pH values is demonstrated in figure 4(b). Furthermore, the encryption and decryption of the letters 'CUHK' (figure 4(c)) and 'USTC' (figure 4(d)) were also realized.

The resultant Janus microactuators could be applied in microobject trapping, which is in high demanded in the fields of chemical analysis [38] and biomedical devices [39]. Although many interesting works have been published on

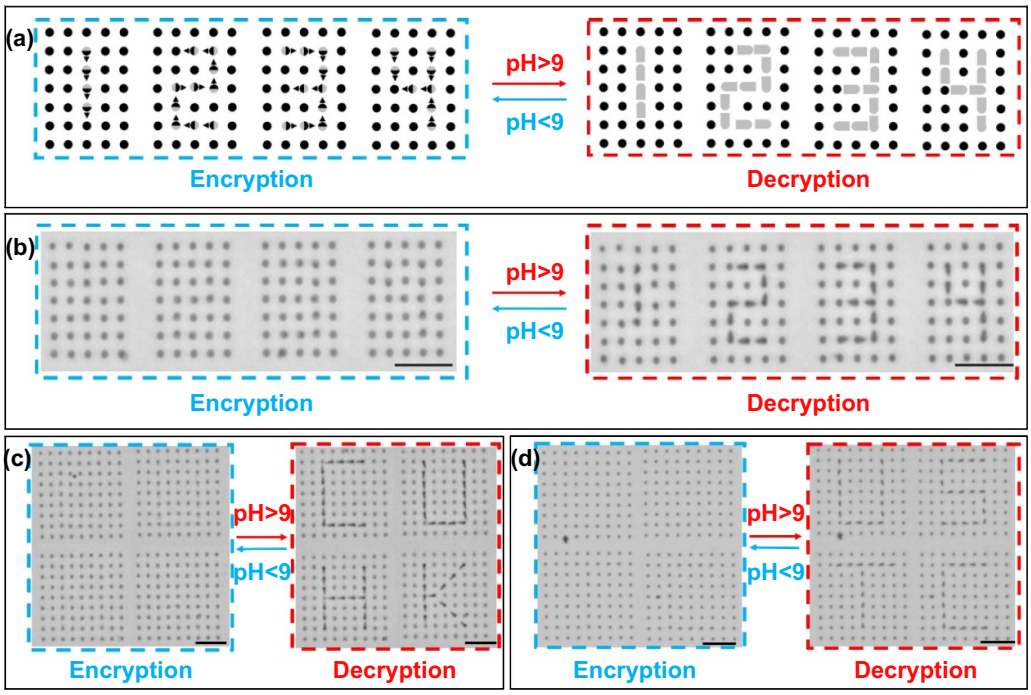

Figure 4. Applications of Janus microactuators in information encryption/decryption. (a) Conceptional design of encryption (left) and decryption (right) of Arabic numerals '1234'. (b)–(d) Optical micrographs of encryption (left) and decryption (right) of (b) '1234', (c) 'CUHK' and (d) 'USTC'. Scale bars: 15 μm.

microobject trapping, simple and tunable microgrippers are still in demand [16, 17, 40, 41]. The trapping process is sketched in figure 5(a), the solvent containing microobjects is dropped on the sample for trapping particles (figure 5(a I)). The claw-like structures containing four micropillars provide an open space that the microobject can enter with ease when pH < 9 (figure 5(a II)). When pH > 9, these Janus microactuators bend and the claw-like structure grasps the microspheres tightly (figure 5(a III)), which can withstand a certain degree of shaking and external force. Figures 5(b) and (d) show that a PS (polystyrene) microsphere with a diameter of 10 μm can enter the open space with a pitch of 11 μm and escape if it is subjected to upward force. When we raise the pH value of the aqueous solution above 9, the microsphere is caught tightly by the four bent microactuators (figure 5(f)). Flow forces were exerted on the microobject in different directions to test the stability of the trapping. The microsphere remained tightly trapped under upward (figure 5(g)) and leftward (figure 5(h)) forces.

3. Conclusion

In summary, we propose a simple and flexible dual-scanning strategy for fabricating pH-driven geometry-switchable Janus micropillars. By utilizing the light scattering from the printed structure, heterogeneity forms with an individual material, and the same processing parameters. This method differs from current strategies of constructing Janus structures, which rely on different materials, multi-step manufacturing, and/or different processing parameters. Changes in pH values triggers the bending effect of these Janus micropillars, resulting in a microactuator with fast response time (∼0.2 s). By taking full advantage of the flexibility of laser writing, the number of pillars, spatial location, and bending direction can be easily controlled, leading to a variety of dynamic ordered patterns. The resultant Janus microactuators hold potential in information encryption/decryption and microparticle capture, as demonstrated with the proof-of-concept experiments. In the future, multi-foci and spatial light modulation, which can significantly increase the processing efficiency of laser direct writing [42, 43], can also be employed in the fabrication of such pH-driven Janus microactuators. The combination of fs laser direct writing and environmentally sensitive smart materials opens up a new avenue to fabricate functional microactuators with great scalability and flexibility toward numerous applications in smart display, intelligent sensor, microobject manipulation, filtration, and transportation.

4. Experimental

4.1. Preparation of the hydrogel precursor

Firstly, 0.8 ml of acrylic acid (99%), 1.6 g of N-isopropylacrylamide (98%), and 0.15 g of polyvinylpyrrolidone (average Mw ∼1 300 000) were combined in 1 ml of ethyl lactate (98%), and then stirred to dissolve completely. Then, 2.5 ml of the solution was mixed with 0.5 ml of dipentaerythritol hexaacrylate (98%), 0.5 ml of triethanolamine (99%), and 100 μl of 4,4′bis(diethylamino) benzophenone/N,N-dimethylformamide solution (20 wt%). The solution was stirred overnight to ensure each component was evenly mixed. The prepared hydrogel precursor was

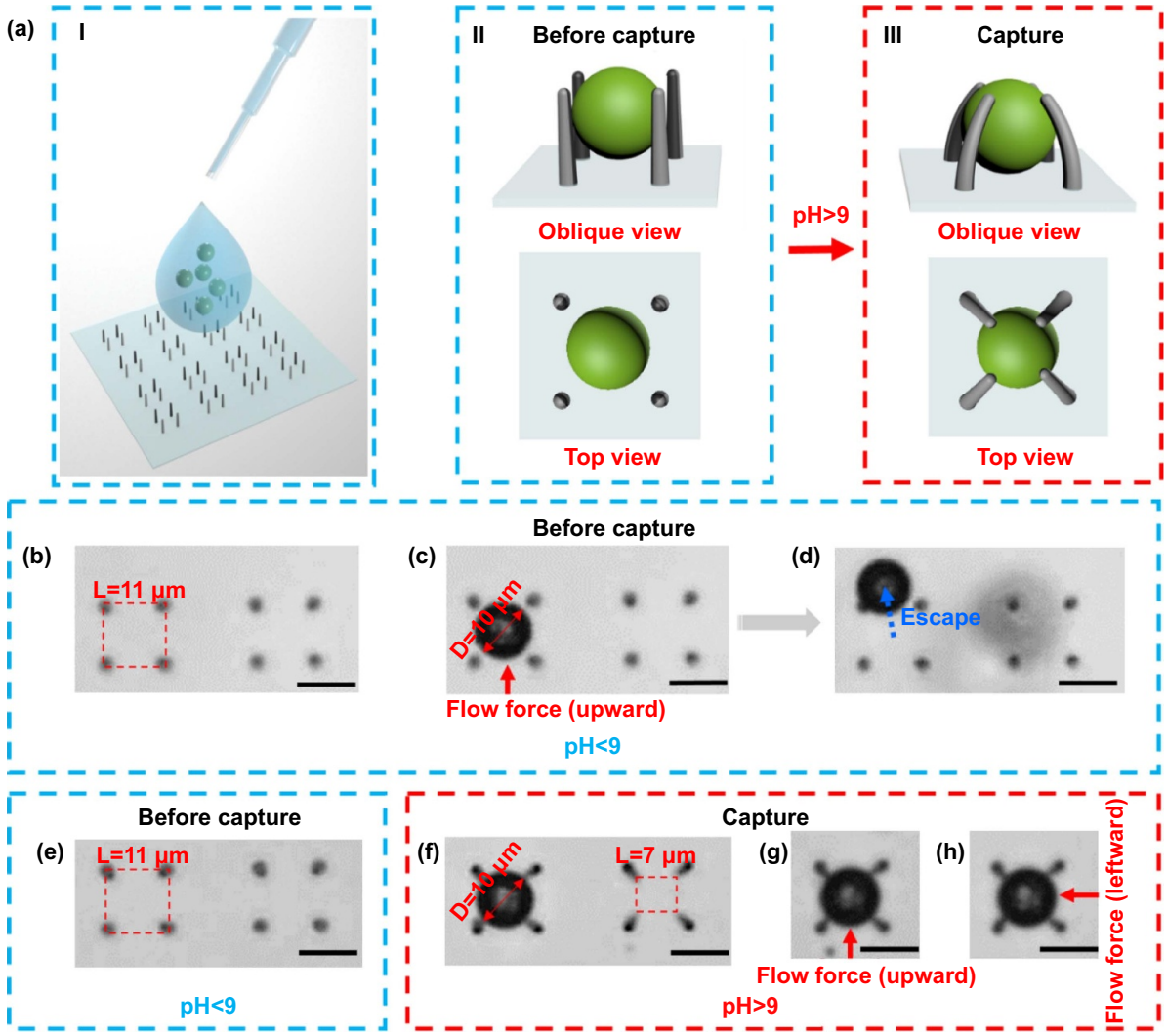

Figure 5. Demonstration of the microparticle trapping. (a) Illustration of the concept of microobject trapping. (b)–(d) PS microsphere (10 μm) can enter and overflow the open space with pitch of 11 μm, which was composed of four straight micropillars when pH < 9. (e) Open space with pitch of 11 μm before capture. (f)–(h) A trapped microsphere that can withstand extra upward and leftward forces. Scale bars: 10 μm.

kept in yellow light conditions to avoid unnecessary light exposure.

4.2. Fabrication of Janus micropillars actuator

A Ti:sapphire fs laser system (Chameleon Vision-S, Coherent Inc., USA) was used for direct laser writing. The fs-laser had a central wavelength of 800 nm, pulse width of 75 fs, and repetition rate of 80 MHz, respectively. A 50× objective (Olympus, NA = 0.8) was used to focus the laser beam inside the hydrogel. The laser power was 45 mW and the exposure time of single point was 70 ms, while the focus was an ellipsoid with the size ~1.2 μm × 0.5 μm × 0.5 μm. The exposure threshold of the material was ~30 mW. Improper energy could cause unsuccessful results. Over-exposure can occur if the power is too high, resulting in disordered structures, while exposure with insufficient power will make the expansion difference between opposite sides of pillar too small to trigger the pH response. A nanotranslation stage (PI, E545) was used to accurately determine the relative position of the sample and focus. The step pitch (x, y, z) of stage was set at 0.15 μm, 0.15 μm, and 0.4 μm. Each vertical scanning process follows a point-to-point scanning manner. The distance between adjacent points was 0.4 μm, and the exposure time of each point was 70 ms. The stage translation time between adjacent points was less than 1 ms. Therefore, the scanning velocity in the vertical direction can be calculated as ~0.4 μm/70 ms = 5.7 μm s^{-1}. After being polymerized by the fs-laser, the sample was developed in isopropanol for 15 min to remove the unpolymerized part. A sodium hydroxide solution and diluted hydrochloric acid were dropped on the sample to change the pH value of the environment. The microchannel was prepared manually under a microscope by attaching two glass slides (the depth was ~170 μm) on a glass substrate. The channel width was adjusted with copper wire (with a diameter of ~200 μm). The channels were prepared by dropping

water on substrate and carefully pressing the slides together. Then, the hydrogel resin was dropped into the channel for laser manufacturing.

4.3. Sample characterization and image acquisition

The structures were deposited with ∼10 nm of gold and subsequently investigated using SEM (ZEISS EVO18) at an accelerating voltage of 10 keV. The optical images were obtained from a Leica fluorescence microscope (LEICA DMI3000 B). In the microfluidic experiment, the change of pH was realized by the spontaneous diffusion of aqueous solutions with different pH values. It should be noted that, because the hydrogel is very soft, microactuators may be washed down by solution flow or touch each other too tightly. A few actuators in the array may not recovery their upright positions in the pH cycles.

4.4. Capture of microspheres

Commercialized PS particles (Tianjin Saierqun Technology Co. Ltd, China) with a diameter of 10 μm were mixed in water at a concentration of about 10–4 g ml^{-1}. For the particle-trapping experiment, the solvent containing microspheres was dropped on the sample. Directional forces were generated by dropping water at different positions around the sample.

Acknowledgments

Z X Lao thanks the Hong Kong Scholar Program (XJ2018035) for their financial support. This work was supported by Research Grants Council of Hong Kong (No. JLFS/E-402/18) and National Natural Science Foundation of China (No. 51805509). We acknowledge the Experimental Center of Engineering and Material Sciences at USTC for their help with fabricating and characterizing the sample materials. This work was partly carried out at the USTC Center for Micro and Nanoscale Research and Fabrication. None of the authors declare conflicts of interest.

Author contributions

D D Jin, L Zhang prepared the material; Z X Lao, R Sun and L Zhang designed the experiments; Z X Lao, R Sun, Z G Ren, C Xin performed the experiments; all authors analyzed the data; Z X Lao, R Sun, Y C Zhang, S J Jiang and Y Y Zhang drew the figures; Z X Lao, R Sun, D D Jin and L Zhang wrote the paper.

ORCID iD

Li Zhang https://orcid.org/0000-0003-1152-8962

References

[1] Dawson C, Vincent J F V and Rocca A M 1997 How pine cones open *Nature* **390** 668
[2] Allen J J, Bell G R R, Kuzirian A M and Hanlon R T 2013 Cuttlefish skin papilla morphology suggests a muscular hydrostatic function for rapid changeability *J. Morphol.* **274** 645–56
[3] Forterre Y, Skotheim J M, Dumais J and Mahadevan L 2005 How the Venus flytrap snaps *Nature* **433** 421–5
[4] Elbaum R, Zaltzman L, Burgert I and Fratzl P 2007 The role of wheat awns in the seed dispersal unit *Science* **316** 884–6
[5] Vandenbrink J P, Brown E A, Harmer S L and Blackman B K 2014 Turning heads: the biology of solar tracking in sunflower *Plant Sci.* **224** 20–26
[6] Zhang Y C *et al* 2018 Localized self-growth of reconfigurable architectures induced by a femtosecond laser on a shape-memory polymer *Adv. Mater.* **30** 1803072
[7] Mu J K, Hou C Y, Wang H Z, Li Y G, Zhang Q H and Zhu M F 2015 Origami-inspired active graphene-based paper for programmable instant self-folding walking devices *Sci. Adv.* **1** e1500533
[8] Felton S, Tolley M, Demaine E, Rus D and Wood R 2014 Applied origami. A method for building self-folding machines *Science* **345** 644–6
[9] Stoychev G, Puretskiy N and Ionov L 2011 Self-folding all-polymer thermoresponsive microcapsules *Soft Matter* **7** 3277–9
[10] Bassik N, Abebe B T, Laflin K E and Gracias D H 2010 Photolithographically patterned smart hydrogel based bilayer actuators *Polymer* **51** 6093–8
[11] Liu Y, Boyles J K, Genzer J and Dickey M D 2012 Self-folding of polymer sheets using local light absorption *Soft Matter* **8** 1764–9
[12] Leong T G, Lester P A, Koh T L, Call E K and Gracias D H 2007 Surface tension-driven self-folding polyhedra *Langmuir* **23** 8747–51
[13] Na J H, Evans A A, Bae J, Chiappelli M C, Santangelo C D, Lang R J, Hull T C and Hayward R C 2015 Programming reversibly self-folding origami with micropatterned photo-crosslinkable polymer trilayers *Adv. Mater.* **27** 79–85
[14] Duan H G and Berggren K K 2010 Directed self-assembly at the 10 nm scale by using capillary force-induced nanocohesion *Nano Lett.* **10** 3710–6
[15] Lao Z X, Hu Y L, Zhang C C, Yang L, Li J W, Chu J R and Wu D 2015 Capillary force driven self-assembly of anisotropic hierarchical structures prepared by femtosecond laser 3D printing and their applications in crystallizing microparticles *ACS Nano* **9** 12060–9
[16] Lao Z X, Pan D, Yuan H W, Ni J C, Ji S Y, Zhu W L, Hu Y L, Li J W, Wu D and Chu J R 2018 Mechanical-tunable capillary-force-driven self-assembled hierarchical structures on soft substrate *ACS Nano* **12** 10142–50
[17] Hu Y L, Lao Z X, Cumming B P, Wu D, Li J W, Liang H Y, Chu J R, Huang W H and Gu M 2015 Laser printing hierarchical structures with the aid of controlled capillary-driven self-assembly *Proc. Natl Acad. Sci. USA* **112** 6876–81
[18] Lao Z X, Hu Y L, Pan D, Wang R Y, Zhang C C, Ni J C, Xu B, Li J W, Wu D and Chu J R 2017 Self-sealed bionic long microchannels with thin walls and designable nanoholes prepared by line-contact capillary-force assembly *Small* **13** 1603957
[19] Lao Z X *et al* 2020 Nanogap plasmonic structures fabricated by switchable capillary-force driven self-assembly for localized sensing of anticancer medicines with microfluidic SERS *Adv. Funct. Mater.* **30** 1909467
[20] Loget G, Roche J and Kuhn A 2012 True bulk synthesis of janus objects by bipolar electrochemistry *Adv. Mater.* **24** 5111–6
[21] Hu S H and Gao X H 2010 Nanocomposites with spatially separated functionalities for combined imaging and magnetolytic therapy *J. Am. Chem. Soc.* **132** 7234–7

[22] Yan S G *et al* 2018 Unidirectional self-transport of air bubble via a Janus membrane in aqueous environment *Appl. Phys. Lett.* **113** 261602
[23] Zhang Z *et al* 2017 A Janus oil barrel with tapered microhole arrays for spontaneous high-flux spilled oil absorption and storage *Nanoscale* **9** 15796–803
[24] Martella D, Nocentini S, Nuzhdin D, Parmeggiani C and Wiersma D S 2017 Photonic microhand with autonomous action *Adv. Mater.* **29** 1704047
[25] Han H *et al* 2017 Bioinspired geometry-switchable janus nanofibers for eye-readable H_2 sensors *Adv. Funct. Mater.* **27** 1701618
[26] Han D D, Zhang Y L, Liu Y, Liu Y Q, Jiang H B, Han B, Fu X Y, Ding H, Xu H L and Sun H B 2015 Bioinspired graphene actuators prepared by unilateral UV irradiation of graphene oxide papers *Adv. Funct. Mater.* **25** 4548–57
[27] Zhang X B *et al* 2014 Photoactuators and motors based on carbon nanotubes with selective chirality distributions *Nat. Commun.* **5** 2983
[28] Kim T I, Jeong H E, Suh K Y and Lee H H 2009 Stooped nanohairs: geometry-controllable, unidirectional, reversible, and robust gecko-like dry adhesive *Adv. Mater.* **21** 2276–81
[29] Ma H, Hou J W, Wang X W, Zhang J, Yuan Z Q, Xiao L, Wei Y, Fan S S, Jiang K L and Liu K 2017 Flexible, all-inorganic actuators based on vanadium dioxide and carbon nanotube bimorphs *Nano Lett.* **17** 421–8
[30] Huang T Y, Huang H W, Jin D D, Chen Q Y, Huang J Y, Zhang J and Duan H L 2020 Four-dimensional micro-building blocks *Sci. Adv.* **6** eaav8219
[31] Hu Y L *et al* 2020 Chiral assemblies of laser-printed micropillars directed by asymmetrical capillary force *Adv. Mater.* **32** 2002356
[32] Ma J N, Zhang Y L, Han D D, Mao J W, Chen Z D and Sun H B 2020 Programmable deformation of patterned bimorph actuator swarm *Natl Sci. Rev.* **7** 775–85
[33] Jin D D, Chen Q Y, Huang T Y, Huang J Y, Zhang L and Duan H L 2020 Four-dimensional direct laser writing of reconfigurable compound micromachines *Mater. Today* **32** 19–25
[34] Zhang Y L, Tian Y, Wang H, Ma Z C, Han D D, Niu L G, Chen Q D and Sun H B 2019 Dual-3D femtosecond laser nanofabrication enables dynamic actuation *ACS Nano* **13** 4041–8
[35] Li R *et al* 2020 Stimuli-responsive actuator fabricated by dynamic asymmetric femtosecond bessel beam for *in situ* particle and cell manipulation *ACS Nano* **14** 5233–42
[36] Hu Y L *et al* 2020 Botanical-inspired 4D printing of hydrogel at the microscale *Adv. Funct. Mater.* **30** 1907377
[37] Gupta P, Vermani K and Garg S 2002 Hydrogels: from controlled release to pH-responsive drug delivery *Drug Discovery Today* **7** 569–79
[38] Xu B, Shi Y, Lao Z X, Ni J C, Li G Q, Hu Y L, Li J W, Chu J R, Wu D and Sugioka K 2018 Real-time two-photon lithography in controlled flow to create a single-microparticle array and particle-cluster array for optofluidic imaging *Lab Chip* **18** 442–50
[39] Martella D, Nocentini S, Parmeggiani C and Wiersma D S 2019 Self-regulating capabilities in photonic robotics *Adv. Mater. Technol.* **4** 1800571
[40] Leong T G, Randall C L, Benson B R, Bassik N, Stern G M and Gracias D H 2009 Tetherless thermobiochemically actuated microgrippers *Proc. Natl Acad. Sci. USA* **106** 703–8
[41] Breger J C, Yoon C, Xiao R, Kwag H R, Wang M O, Fisher J P, Nguyen T D and Gracias D H 2015 Self-folding thermo-magnetically responsive soft microgrippers *ACS Appl. Mater. Interfaces* **7** 3398–405
[42] Ni J C, Wang C W, Zhang C C, Hu Y L, Yang L, Lao Z X, Xu B, Li J W, Wu D and Chu J R 2017 Three-dimensional chiral microstructures fabricated by structured optical vortices in isotropic material *Light Sci. Appl.* **6** e17011
[43] Hu Y L, Feng W F, Xue C, Lao Z X, Ji S Y, Cai Z, Zhu W L, Li J W, Wu D and Chu J R 2020 Self-assembled micropillars fabricated by holographic femtosecond multi-foci beams for *in situ* trapping of microparticles *Opt. Lett.* **45** 4698–701